NANO LETTERS

2006
Vol. 6, No. 1
24−28

Novel Carbon-Doped TiO_2 Nanotube Arrays with High Aspect Ratios for Efficient Solar Water Splitting

Jong Hyeok Park, Sungwook Kim, and Allen J. Bard*

Department of Chemistry and Biochemistry, The University of Texas at Austin, Austin, Texas 78712

Received September 8, 2005; Revised Manuscript Received November 1, 2005

ABSTRACT

The photocatalytic splitting of water into hydrogen and oxygen using solar light is a potentially clean and renewable source for hydrogen fuel.[1,2] There has been extensive investigation into metal-oxide semiconductors such as TiO_2, WO_3, and Fe_2O_3, which can be used as photoanodes in thin-film form.[3−5] Of the materials being developed for photoanodes, TiO_2 remains one of the most promising because of its low cost, chemical inertness, and photostability.[6] However, the widespread technological use of TiO_2 is hindered by its low utilization of solar energy in the visible region. In this study, we report the preparation of vertically grown carbon-doped TiO_2 ($TiO_{2-x}C_x$) nanotube arrays with high aspect ratios for maximizing the photocleavage of water under white-light irradiation. The synthesized $TiO_{2-x}C_x$ nanotube arrays showed much higher photocurrent densities and more efficient water splitting under visible-light illumination (> 420 nm) than pure TiO_2 nanotube arrays. The total photocurrent was more than 20 times higher than that with a P-25 nanoparticulate film under white-light illumination.

The photocatalytic effect in solid-state catalysis occurs when the electron−hole pair (e^-h^+) created by photon absorption can interact with molecules close to the catalyst surface. Although TiO_2 has several advantages as described above, it has two critical limitations. The first is that exciton creation, the e^-h^+ precursor, is achieved only with UV light, rendering the use of solar irradiation inefficient because of the wide band gap of the most common polymorphic forms of TiO_2 (3.0 eV for rutile and 3.2 eV for anatase).[7] Second, the large band-gap oxide semiconductors, such as n-type TiO_2 or WO_3 employed in photoelectrochemical devices, often have short exciton diffusion lengths, so it is mainly the carriers generated within the space charge layer that contribute to the photocurrent.[8] To maximize the water splitting efficiency of a TiO_2 photoanode, one would like (1) a narrower band gap to utilize visible-light energy, (2) a high contact area with the electrolyte to increase the splitting of the e^-h^+ pairs, and (3) a thicker film to increase the total absorption of solar light (Figure 1).

Narrowing of the band gap has been reported in microcrystalline TiO_2 films doped with N, C, and S,[9−11] with carbon-doped TiO_2 as one of the best in terms of band-gap width. The most common method for preparing a carbon-doped TiO_2 film is by direct oxidation of the Ti metal in the flame of a burner.[12−14] Khan et al. reported quantitative results on a new carbon-doped rutile photoanode for the photosplitting of water, but there is still disagreement about its solar-to-hydrogen conversion efficiency.[15−17]

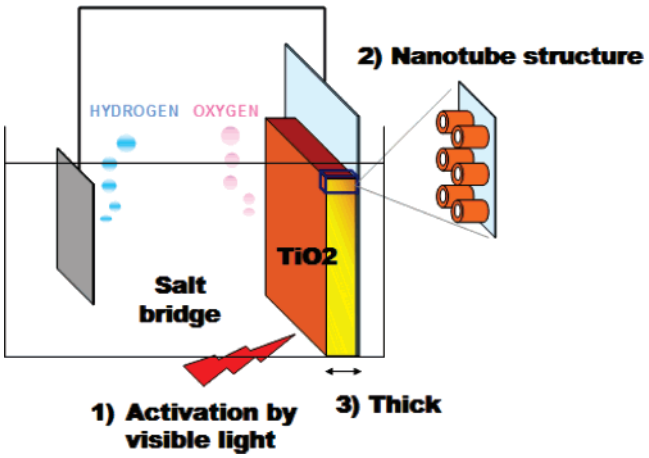

Figure 1. Schematic structure of the TiO_2 photoanode to optimize its photocatalytic activity for water splitting. (1) TiO_2 should absorb a considerable fraction of the solar spectrum. (2) All electron and hole pairs on excitation should be located within the space charge layer (5−200 nm) at the electrolyte/semiconductor interface. (3) To maximize absorption of solar photons, a thicker TiO_2 photoanode is desirable.

Although these carbon-doped TiO_2 films exhibited enhanced photocurrents under visible-light illumination, their morphologies could not be controlled well by the flame oxidation method. Recently, our group investigated the relationship between water-splitting behavior and the TiO_2

* To whom correspondence should be addressed. E-mail: ajbard@mail.utexas.edu.

10.1021/nl051807y CCC: $33.50
Published on Web 12/10/2005

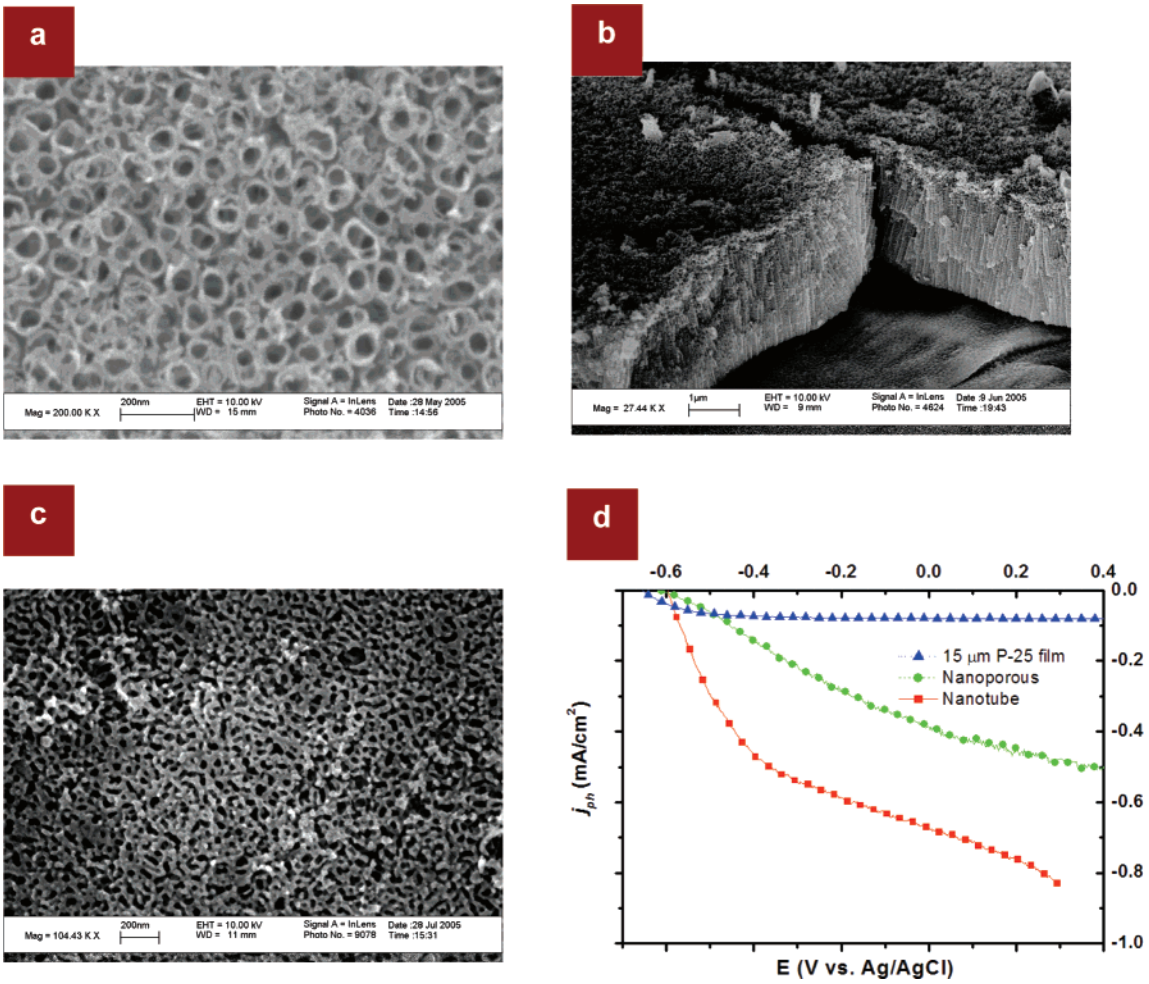

Figure 2. Relationship between photocurrent and morphology. (a) SEM image, top view of TiO_2 nanotube arrays of ~3 μm length. (b) Cross-sectional SEM image of TiO_2 nanotube arrays of ~3 μm length (45° tilted image from top view). (c) SEM image, top view of nanoporous TiO_2 with ~3 μm thickness. (d) Variation of photocurrent density vs measured potential for three different TiO_2 photoanodes in 1 M KOH electrolyte.

morphology. The water-splitting photocurrent was found to depend on the aspect ratio of the TiO_2 nanotube with 3.3-μm-length TiO_2 nanotube arrays producing a photoanodic response more than 10 times that of a 15-μm-thick TiO_2 nanoparticle (P-25) film under the same illumination conditions.

TiO_2 nanotube arrays with high aspect ratios were grown from a Ti substrate (0.25-mm-thick, Aldrich) by anodization in an electrolyte of 1 M $(NH_4)H_2PO_4$ + 0.5 wt % NH_4F.[18] A two-electrode electrochemical setup consisting of the Ti substrate anode and a Pt wire cathode was used. The morphology depended strongly on the applied voltage. To obtain well-organized TiO_2 nanotubes, we applied about 15 V. As shown in Figure 2c, anodizing the Ti substrate at 20 V only produced a porous TiO_2 film. The anodized Ti substrate was annealed at 450 °C in oxygen for 1 h with heating and cooling rates of 2 °C/min to convert the amorphous phase to a crystalline one. To introduce the carbon dopant into the TiO_2 nanotube arrays, they were annealed at high temperature (500 to 800 °C) under controlled CO gas flow.

Figure 2 (a and b) shows scanning electron microscope (SEM) images of a TiO_2 nanotube array with a ~3 μm length. The pore diameter was about 70 nm, and the wall thickness was 20 nm. Figure 2d shows a comparison of the photocurrent density vs applied potential curves for two undoped TiO_2 photoanodes with different morphologies and one commercial P-25 TiO_2 photoanode under Xe lamp irradiation (~100 mW/cm^2). At 0.4 V, the photocurrent density of a TiO_2 nanotube array (~2 μm length) was more than 60% greater than the value for a nanoporous TiO_2 film with a similar thickness. This suggests that TiO_2 nanotube arrays can harvest solar light more effectively than photoanodes with an irregular structure under the same illumination. In addition, the TiO_2 nanotubular structure also shows a steeper increase in the photocurrent with applied potential. Thus with the TiO_2 nanotubes, e^-h^+ pairs induced by photon absorption split more readily compared to a nanoporous structure. The nanotube arrays also produced a photoanodic response more than 10 times higher than a 15-μm-thick TiO_2 (P-25) nanoparticle flat film because incident photons are more effectively absorbed on a flat electrode, probably because of an increased light penetration depth and better scattering within a regular pore structure.[19] In addition, the induced e^-h^+ pairs in the TiO_2 nanotubular structure might be extracted more efficiently than the 15-μm-thick TiO_2 (P-

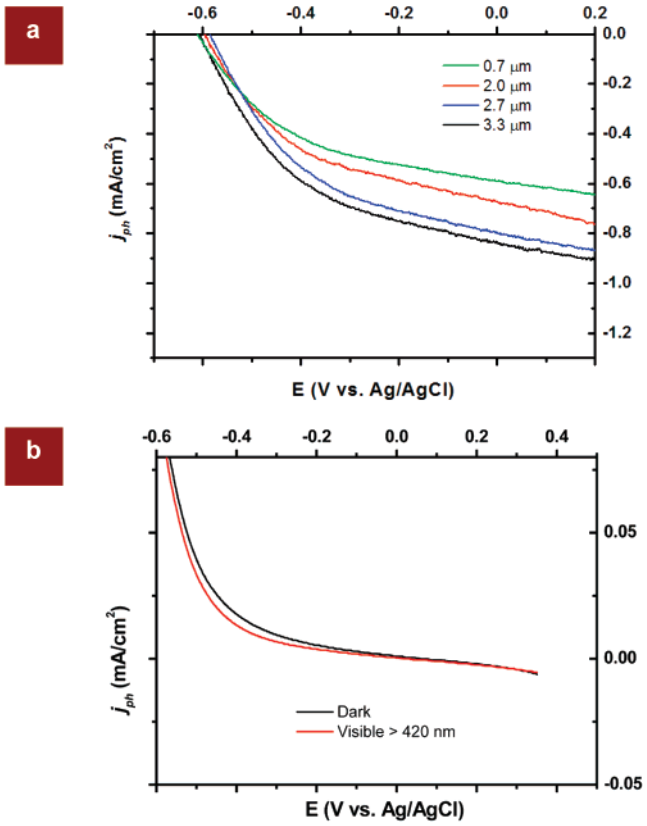

Figure 3. (a) Variation of photocurrent density vs measured potential as a function of TiO_2 nanotube length. (b) Typical current−potential characteristics of the TiO_2 nanotube array in the dark and under visible-light (>420 nm) illumination.

25) nanoparticle flat film because of the high contact area between the photocatalyst and electrolyte.

Figure 3a shows the photocurrent−potential dependence of several TiO_2 nanotube arrays prepared with different tube lengths controlled by anodization times. The open circuit photopotential was −0.6 V/Ag/AgCl, independent of anodization duration. However, the magnitude of the photocurrent density at more positive potentials was a function of the tube length. A theoretical expression of photocurrent density that includes the charge transfer at the photoelectrode−solution interface is useful in understanding this behavior.[5] When the tube length increases, more light is absorbed and the photocurrent density increases as with other semiconductor films. However, for flat films, when the thickness of the film exceeds some critical point, recombination of photogenerated electrons and holes dominate because of the decreased electric field within the film. An increase in bulk recombination and surface recombination rates produces a smaller photocurrent. The photocurrent does not increase further, even when the film can absorb more photons from the incident solar light. This smaller photocurrent can also be explained by a combination of increased resistance and a higher recombination rate of the generated electrons and holes due to reduction in the electric field in the thicker film. With the nanotube system, when the tube length increases, more photons are absorbed and, consequently, the photocurrent increases. Even though the tube length increases, the bulk recombination rate and surface recombination rate of photogenerated carriers are still much less than charge-transfer rate at the interface because the TiO_2 nanotube array architecture results in a large effective surface area in close proximity with the electrolyte, thus enabling diffusive transport of photogenerated holes to oxidizable species in the electrolyte. As in Figure 3a, the photocurrent increases as the tube length increases up to 3.3 μm. A maximum conversion efficiency of 0.55% was obtained for nanotube arrays with 3.3-μm tube lengths. Figure 3b shows the photocurrent−potential characteristics of the TiO_2 nanotube array electrodes under visible-light (>420 nm) illumination. The photocurrent is essentially the same as the dark current, showing that there is no photocatalytic activity under visible light for undoped TiO_2 nanotube arrays.

Figure 4a is an SEM image of carbon-doped TiO_2 nanotube arrays annealed at 600 °C under a CO gas flow. No significant morphological change was observed. This thermal treatment did not destroy the nanostructure of the as-prepared TiO_2 nanotube array. X-ray photoelectron spectroscopy (XPS) confirmed enhanced carbon incorporation (Figure 4b). In addition, the color change of the nanotube array upon carbon incorporation demonstrates an effect on their optical response in the visible wavelength range. By adjusting the temperature of heat treatment, the doping concentration of carbon in the TiO_2 nanotube array could be controlled between 8 and 42% (as determined from the XPS peaks). No appreciable signal related to carbide (281.5 eV) was observed, showing that the amount of Ti-bonded carbon was very low.

The photooxidation activity of the $TiO_{2-x}C_x$ nanotube array was evaluated by measuring the photocurrent in 1 M KOH electrolyte. Shown in Figure 5a is the observed photocurrent density of a $TiO_{2-x}C_x$ nanotube array under visible light. The $TiO_{2-x}C_x$ nanotube array showed obvious enhanced photocatalytic activity under visible light compared to undoped TiO_2 nanotubes. The proposed model for visible-light absorption in doped TiO_2 is due to substitution of oxygen by another atom, such as N or C, which results in a mix of N,C2*p* and O2*p* states.[20] Moreover, the total photocurrent under white-light illumination was larger than that of the undoped TiO_2 nanotube array. This shows that the gain from improved visible-light absorption is larger than any loss from reduced photocatalytic activity under UV light absorption.[21]

Optical transitions for crystalline semiconductors can be deduced from the variation of the absorption coefficient near the band edge. For direct band gaps (E_g), the optical absorption near the band edge is given by[22]

$$\alpha = A(h\nu - E_g)^n/h\nu \qquad (1)$$

where A is a constant and n equals 0.5 for an allowed direct transition. The allowed direct transition of an electron from the valence band to the conduction band by light energy is not phonon-assisted and does not require a simultaneous change in momentum.[5] Equation 1 is most appropriate to use when the applied potential is far from the flatband potential. By assuming that the photocurrent (j_{ph}) is proportional to the absorption coefficient, α, the band-gap energy

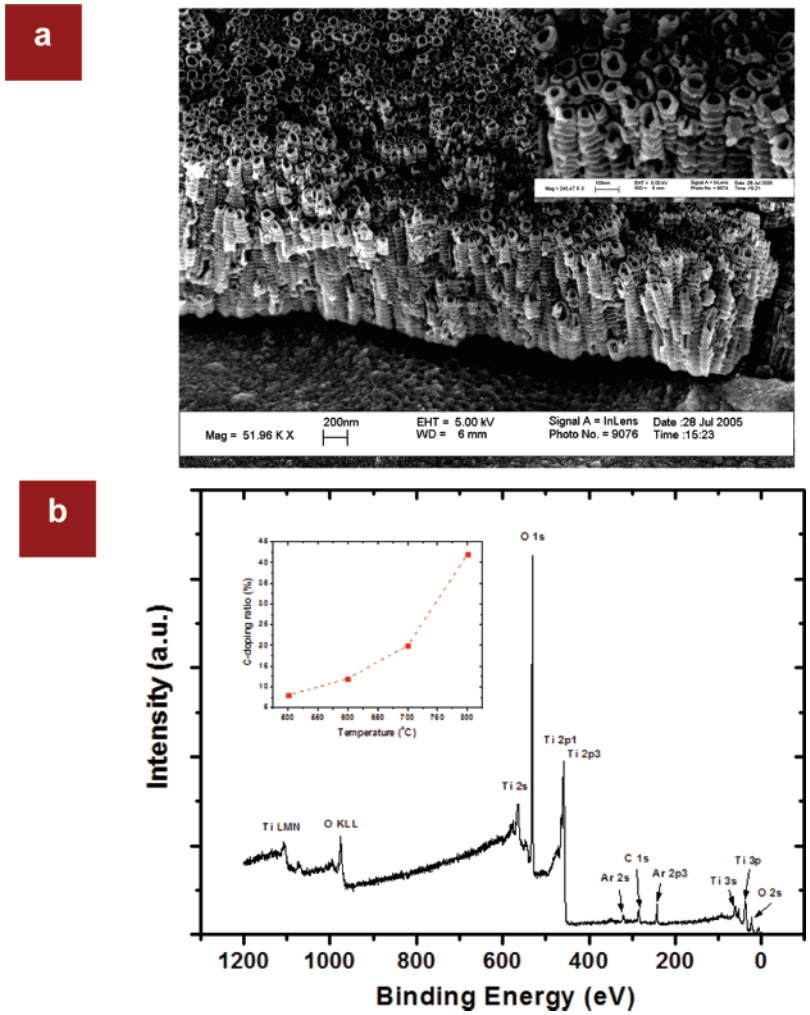

Figure 4. (a) Cross-sectional SEM image of $TiO_{2-x}C_x$ nanotube arrays of ~3 μm length. (b) XPS spectrum of the $TiO_{2-x}C_x$ nanotube array prepared at 500 °C. Before measurement, the sample was sputtered with Ar ions for 1 min. The inset figure shows the carbon doping concentration as a function of heat-treatment temperature.

of the $TiO_{2-x}C_x$ nanotube array was determined from a plot of $(j_{ph}h\nu)^{1/2}$ versus $h\nu$ (Figure 5b). The linear portion of this curve indicates a transition above an optical band-edge and an intercept of about 2.22 eV, (corresponding to the band-gap energy of the $TiO_{2-x}C_x$ nanotube array). This energy is slightly larger than the earlier reported value of ~2 eV.[10]

The role of the doping concentration causing a photocurrent increase was supported by the study of the photocurrent versus annealing temperature. Measurements of the photocurrent were carried out at each annealing step (Figure 5c). Significant changes of the photocurrent occurred up to 600 °C because of the increased activity under visible-light illumination, indicating carbon diffusion and doping was taking place. However, from 700 °C, the photocurrent density decreased, suggesting that higher doping decreases photocatalytic sites. By collecting the gases at the TiO_2 and Pt counter electrode during the photoreaction, we observed a 2.1:1 volume ratio of hydrogen and oxygen.

To confirm that the TiO_2 nanotube structure was the enabling factor in this doping process, we carried out the same experimental protocol with a TiO_2 film of P-25. Following the identical thermal treatment under CO gas flow to produce carbon doping, the photocurrent was still much lower than that of the $TiO_{2-x}C_x$ nanotube array but was slightly higher than the P-25 film without carbon doping.

In conclusion, we have demonstrated significant progress toward the goal of enhancing photocatalytic activity of TiO_2, by using aspect-ratio-controlled TiO_2 nanotube arrays as a starting material for preparing a novel photocatalyst with a smaller band gap. The unique structure of the TiO_2 nanotube array produced by controlling the anodizing conditions favors the incorporation of carbon by heating with CO at temperatures up to 600 °C. This investigation shows that a chemical approach to decreasing the band gap can be combined with the control of morphology to maximize solar energy harvesting. Although in this study, water oxidation on the $TiO_{2-x}C_x$ nanotube array was investigated, the valence band of the semiconductor is more positive than that required for other photoreactions of organic or inorganic species (e.g., alcohol, I^-, Br^-, and SCN^-), so that C-doped TiO_x nanotubes could find use in other applications.

Methods. *Preparation of Photoanode.* Titanium foil was degreased by sonicating in 2-propanol and methanol and then rinsing with deionized water and drying in a nitrogen flow. It was positioned between two plastic substrates and then pressed against an O ring in an electrochemical cell with a

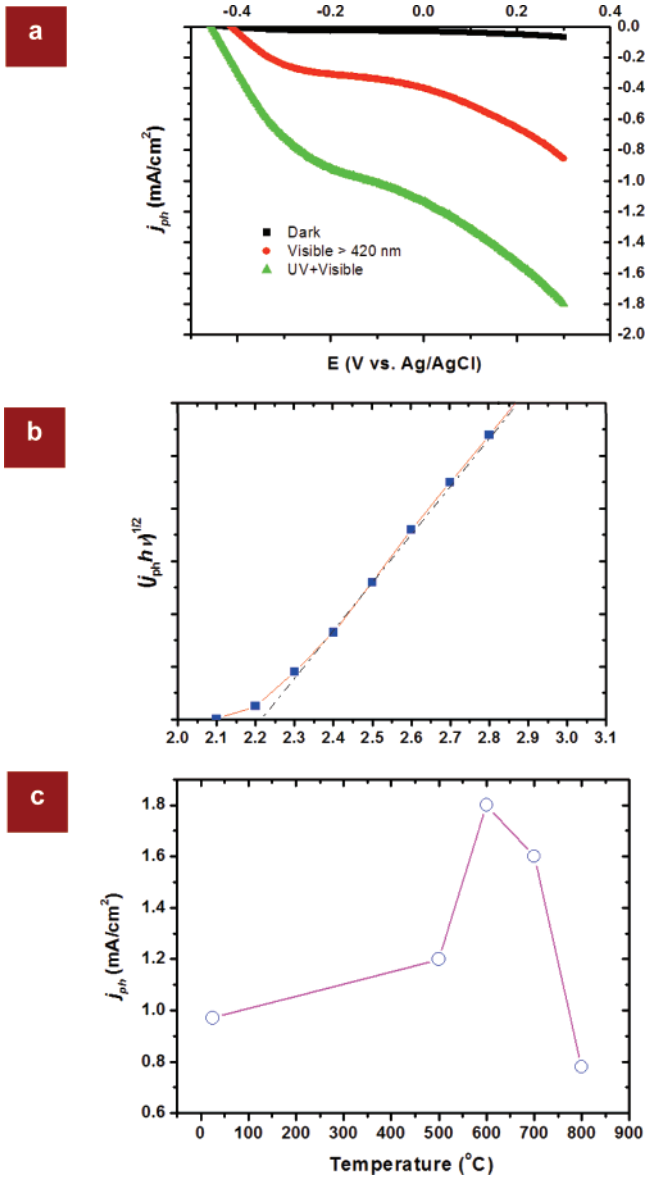

Figure 5. (a) Current−potential characteristics of the $TiO_{2-x}C_x$ nanotube array prepared at 600 °C in the dark and under visible-light and white-light illumination. (b) Band-gap determination of the $TiO_{2-x}C_x$ nanotube array prepared at 600 °C from the $(j_{ph}h\nu)^{1/2}$ vs $h\nu$ plot. (c) Total current density as a function of heat-treatment temperature under white-light illumination.

0.8 cm^2 exposed area. All electrolytes were prepared from reagent-grade chemicals. The anodizing process consisted of a potential ramp from 0 V to a given potential (e.g., 15 V) at a 1 V/s sweep rate followed by holding at the desired applied potential for various times in 1 M $(NH_4)H_2PO_4$ + 0.5 wt % NH_4F.[18] After the preparation of the TiO_2 nanotube array, the samples were rinsed with deionized water and annealed at 450 °C for 1 h. For comparison, a ∼15-μm-thick film of TiO_2 nanoparticles (P-25) was printed on another Ti foil and then sintered at 450 °C for 1 h.

Surface Characterization. Scanning electron microscopy (SEM, LEO 1530) was employed for the structural and morphological characterization of the TiO_2 nanotube array. Chemical compositions of as-prepared samples were characterized by X-ray photoelectron spectroscopy (XPS, PHI 5600 XPS). XPS were performed in an ultrahigh vacuum analysis chamber (base pressure < 1×10^{-6} Pa) equipped with an electrostatic hemispherical analyzer. Before measurement, the samples underwent a surface-cleaning procedure by argon-ion sputtering to remove chemisorbed species.

Electrochemical Characterization. Electrochemical experiments were carried out using a three-electrode configuration with a Pt wire counter electrode and a saturated Ag/AgCl reference electrode (CH instruments, CHI 660). The potential was swept linearly at a scan rate of 50 mV/s. Photoelectrochemical water splitting experiments were conducted in a 1 M KOH electrolyte. The 1 cm^2 working electrode was illuminated with a 2500 W xenon lamp from which infrared wavelengths were removed by an 8-in water filter. The measured light irradiance was 100 mW/cm^2. For visible-light illumination, the light was passed through an optical filter, which cut off wavelengths below 420 nm.

Acknowledgment. Support of this research by the National Science Foundation (CHE 0202136) and partial fellowship support for J.H.P was provided by a Korea Research Foundation Grant (KRF-2004-214-D00266). We thank C. R. Luman for helpful discussions.

References

(1) Bard, A. J.; Fox, M. A. *Acc. Chem. Res.* **1995**, *28*, 141−145.
(2) Bard, A. J. *Science* **1980**, *207*, 139−144.
(3) Fujishima, A.; Honda, K. *Nature* **1972**, *238*, 37.
(4) Santato, C.; Ulmann, M.; Augustynski, J. *J. Phys. Chem. B* **2001**, *105*, 936−940.
(5) Khan, S.; Akikusa, J. *J. Phys. Chem. B* **1999**, *103*, 7184−7189.
(6) Burda, C.; Lou, Y.; Chen, X.; Samia, A. C. S.; Stout, J.; Gole, J. L. *Nano Lett.* **2003**, *3*, 1049−1051.
(7) Bendavid, A.; Martin, P. J.; Jamting, A.; Takikawa, H. *Thin Solid Films* **1999**, *356*, 6−11.
(8) Santato, C.; Ulmann, M.; Augustynski, J. *Adv. Mater.* **2001**, *13*, 511−514.
(9) De Vos, D. E.; Dams, M.; Sels, B. F.; Jacobs, P. A. *Chem. Rev.* **2002**, *102*, 3615−3640.
(10) Barborini, E.; Conti, A. M.; Kholmanov, I.; Piseri, P.; Podesta, A.; Milani, P.; Cepek, C.; Sakho, O.; Macovez, R.; Sancrotti, M. *Adv. Mater.* **2005**, *17*, 1842−1846.
(11) Yu, J. C.; Ho, W.; Yu, J.; Yip, H.; Wong, P. K.; Zhao, J. *Environ. Sci. Technol.* **2005**, *39*, 1175.
(12) Fujishima, A.; Kohayakawa, K.; Honda, K. *J. Electrochem. Soc.* **1975**, *122*, 1487.
(13) Kahn, S. U. M.; Al-Shahry, M.; Ingler, W. B., Jr. *Science* **2002**, *297*, 2243−2245.
(14) Noworyta, K.; Augustynski, J. *Electrochem. Solid State Lett.* **2004**, *7*, E31−E33.
(15) Fujishima, A. *Science* **2003**, *301*, 1673a.
(16) Hagglund, C.; Gratzel, M.; Kasemo, B. *Science* **2003**, *301*, 1673b.
(17) Lackner, K. S. *Science* **2003**, *301*, 1673c.
(18) Ghicov, A.; Tsuchiya, H.; Macak, J. M. *Electrochem. Commun.* **2005**, *7*, 505−509.
(19) Marin, F. I.; Hamstra, M. A.; Vanmaekelbergh, D. *J. Electrochem. Soc.* **1996**, *143*, 1137−1142.
(20) Asahi, R.; Morikawa, T.; Ohwaki, T.; Aoki, K.; Taga, Y. *Science* **2001**, *293*, 269−271.
(21) Torres, G. R.; Lindgren, T.; Lu, J.; Granqvist, C. G.; Lindquist, S. E. *J. Phys. Chem. B* **2004**, *108*, 5995−6003.
(22) Butler, M. A. *J. Appl. Phys.* **1977**, *48*, 1914−1920.

NL051807Y